


RESEARCH ARTICLE

Decreasing brain iron in multiple sclerosis: The difference between concentration and content in iron MRI

Ferdinand Schweser^{1,2}  | Jesper Hagemeyer¹  | Michael G Dwyer^{1,2}  |
Niels Bergsland^{1,3}  | Simon Hametner⁴ | Bianca Weinstock-Guttman⁵ |
Robert Zivadinov^{1,2}

¹Buffalo Neuroimaging Analysis Center, Department of Neurology, Jacobs School of Medicine and Biomedical Sciences, University at Buffalo, The State University of New York, Buffalo, New York

²Center for Biomedical Imaging, Clinical and Translational Science Institute, University at Buffalo, The State University of New York, Buffalo, New York

³IRCCS, Fondazione Don Carlo Gnocchi ONLUS, Milan, Italy

⁴Department of Neuroimmunology, Center for Brain Research, Medical University of Vienna, Vienna, Austria

⁵Jacobs Multiple Sclerosis Center, Department of Neurology, Jacobs School of Medicine and Biomedical Sciences, University at Buffalo, The State University of New York, Buffalo, New York

Correspondence

Ferdinand Schweser, Buffalo Neuroimaging Analysis Center, Department of Neurology, Jacobs School of Medicine and Biomedical Sciences, University at Buffalo, The State University of New York, Buffalo, NY.
Email: schweser@buffalo.edu

Funding information

National Center for Advancing Translational Sciences of the National Institutes of Health, Grant/Award Number: UL1TR001412

Abstract

Increased brain iron concentration is often reported concurrently with disease development in multiple sclerosis (MS) and other neurodegenerative diseases. However, it is unclear whether the higher iron concentration in patients stems from an influx of iron into the tissue or a relative reduction in tissue compartments without much iron. By taking into account structural volume, we investigated tissue iron *content* in the deep gray matter (DGM) over 2 years, and compared findings to previously reported changes in iron *concentration*. 120 MS patients and 40 age- and sex-matched healthy controls were included. Clinical testing and MRI were performed both at baseline and after 2 years. Overall, iron *content* was calculated from structural MRI and quantitative susceptibility mapping in the thalamus, caudate, putamen, and globus pallidus. MS patients had significantly lower iron content than controls in the thalamus, with progressive MS patients demonstrating lower iron content than relapsing–remitting patients. Over 2 years, iron content *decreased* in the DGM of patients with MS, while it tended to increase or remain stable among controls. In the thalamus, decreasing iron content over 2 years was associated with disability progression. Our study showed that temporally increasing magnetic susceptibility in MS should not be considered as evidence for iron influx because it may be explained, at least partially, by disease-related atrophy. Declining DGM iron *content* suggests that, contrary to the current understanding, iron is being removed from the DGM in patients with MS.

KEYWORDS

iron content, longitudinal study, multiple sclerosis, QSM, quantitative susceptibility mapping

1 | INTRODUCTION

Brain iron levels are known to be disturbed in multiple sclerosis (MS) (Filippi et al., 2019; Hagemeyer, Geurts, & Zivadinov, 2012; Zecca, Youdim, Riederer, Connor, & Crichton, 2004). Most studies reported *increased* iron concentrations in the deep gray matter (DGM)

(Stankiewicz, Neema, & Ceccarelli, 2014) and around plaques (Craeliuss, Migdal, Luessenhop, Sugar, & Mihalakis, 1982), and *reduced* iron concentrations within lesions (Haider et al., 2014; Kutzelnigg et al., 2005; Laule et al., 2013; Yao et al., 2012; Yao et al., 2014), in the normal-appearing white matter (WM) (Hametner et al., 2013; Paling et al., 2012; Popescu et al., 2017; Yu et al., 2018), and in the

This is an open access article under the terms of the Creative Commons Attribution-NonCommercial License, which permits use, distribution and reproduction in any medium, provided the original work is properly cited and is not used for commercial purposes.

© 2020 The Authors. *Human Brain Mapping* published by Wiley Periodicals LLC.

thalamus (Bergsland et al., 2018; Burgetova et al., 2017; Khalil et al., 2015; Louapre et al., 2017; Pontillo et al., 2019; Schweser et al., 2018; Uddin, Lebel, Seres, Blevins, & Wilman, 2016; Zivadinov et al., 2018). The literature considers findings of increased region-average iron concentrations as evidence for iron *influx* (Bergsland et al., 2019; Ndayisaba, Kaindlstorfer, & Wenning, 2019; Williams, Buchheit, Berman, & LeVine, 2012), whereas it is less clear how to interpret *reduced* iron concentrations.

Different iron-sensitive MRI techniques (iron-MRI) have been used to assess alterations in iron concentrations; one of the more recent methods is quantitative susceptibility mapping (QSM) (Burgetova et al., 2017; Hagemeyer et al., 2018; Langkammer et al., 2013; Schweser et al., 2018; Zivadinov et al., 2018). To date, most QSM-based studies in MS patients employed cross-sectional study designs. Recently, the first longitudinal QSM study in MS investigated the evolution of iron concentrations over 2 years, showing that magnetic susceptibility increased in the caudate nucleus, while it decreased in the thalamus (Hagemeyer et al., 2018). This finding was consistent with a previous longitudinal R_2^* -based study (Khalil et al., 2015).

Measurements obtained with QSM in the DGM are highly correlated with post mortem tissue iron concentrations (Langkammer et al., 2012; Stüber, Pitt, & Wang, 2016). Hence, a change in tissue magnetic susceptibility $\Delta\chi$, as measured with QSM, can be expressed as:

$$\Delta\chi = \hat{\chi}_{Fe} \cdot \Delta c_{Fe} \quad (1)$$

where Δc_{Fe} is the change in the local tissue nonheme iron *mass concentration* (the mass of iron *per unit of volume*) and $\hat{\chi}_{Fe}$ is a proportionality constant that depends on the effective magnetic moment of the iron complexes in the tissue (Langkammer et al., 2012). A similar

relationship holds for other iron-sensitive MRI techniques, such as R_2^* mapping (Langkammer et al., 2010; Taege et al., 2019).

The literature has widely overlooked that a decline in the volume of a structure causes an increase in the observed region-average iron concentration unless the regional iron *content* declines proportionally to the volume, and vice versa (Hernández-Torres et al., 2019). In general, the impact of atrophy on the iron concentration depends on the *type of cells* that are affected by the underlying pathological process and *how* the pathological process affects these cells. Figure 1 schematically illustrates different scenarios in a two-compartment model of iron-containing and iron-free cells. As a thought experiment, assume a pathological process causes the loss of a certain percentage of *iron-free* cells but neither directly nor indirectly affects iron homeostasis. In this hypothetical scenario, the concentration, or: density, of the remaining iron-laden cells *increases* (Figure 1a,e, Table 3; constant iron content). The thought experiment illustrates that increased iron concentration on iron-MRI *cannot* be considered as evidence of an involvement of iron or iron-containing cells in the pathology without adequate consideration of simultaneously occurring changes in the local tissue volume.

Several neurodegenerative diseases, including MS (Bergsland et al., 2012), are associated with substantial atrophy of the DGM. However, most previous clinical studies that employed iron MRI in these diseases did not adequately account for structural atrophy. Hence, there is a high likelihood that the increased iron *concentrations* reported in these studies (Connor, Snyder, Arosio, Loeffler, & le Witt, 1995; Hagemeyer et al., 2012), but also in studies of healthy aging (Bilgic, Pfefferbaum, Rohlfing, Sullivan, & Adalsteinsson, 2012; Hagemeyer et al., 2013), were at least partially driven by atrophy of iron-free or low-iron tissue compartments.

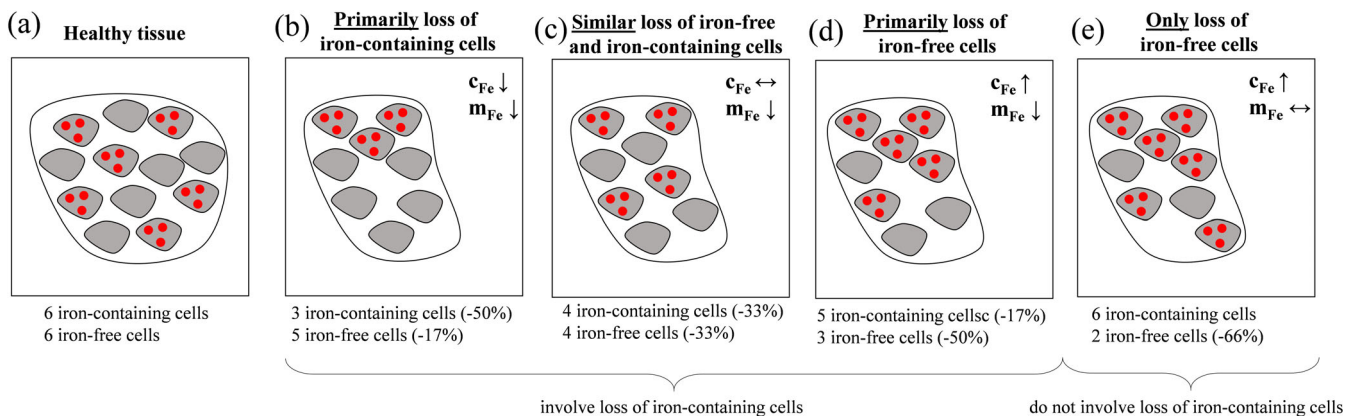


FIGURE 1 Schematic illustration of different cellular realizations of regional atrophy. (a) Healthy tissue model with the same number of iron-containing and iron-free cells. Panels (b–e) show atrophied tissue models characterized by a reduction in the number of cells by one-third. (b) Atrophic mechanism characterized by the removal of primarily iron-laden cells. (c) Iron-containing and iron-free cells are similarly affected by atrophic mechanisms. (d) Primarily iron-free cells are lost. (e) Only iron-free cells are lost. This schematic does not include scenarios in which iron influx occurs, or iron is removed from iron-containing cells (see Table 3). The schematic also does not include scenarios in which iron is transferred between cell-types (e.g., released by iron-containing cells and then taken up by iron-free cells) because such an iron transfer would not affect the bulk tissue magnetic susceptibility (Taege et al., 2019). Furthermore, the conclusions about changes in iron concentration and content would be similar if the “iron-free” cells in the schematic were not completely iron-free but contained considerably less iron than the “iron-containing” cells. In the deep gray matter (DGM), “iron-containing” cells represent oligodendrocytes, and “iron-free” cells represent all other cellular components including neurons and neuropil that have a considerably lower iron content than oligodendrocytes

Recently, Hernández-Torres et al. (2019) estimated regional iron content for the first time from R_2^* values and structural volumes of patients with MS compared to controls in a cross-sectional study. While the study suggested no differences in iron content between patients and controls in putamen and globus pallidus, it found lower iron content in the patients' thalamus and caudate. However, since the physiological meaning of *iron content* is yet unclear, interpretation of these cross-sectional findings was challenging. Linking alterations in these metrics to the underlying mechanisms of disease progression requires the temporal dynamics of iron content and iron concentration.

In the present work, we re-analyzed data presented in our recently published 2-year longitudinal study on magnetic susceptibility in MS (Hagemeier et al., 2018). Combining the susceptibility values with structural volumes, we estimated changes in the *content* of regional tissue iron in milligrams (mg). We hypothesized that tissue atrophy can explain increasing iron concentrations in the DGM of patients with MS and that an assessment of the structural iron content reveals a decrease in the iron load, similar to *ex vivo* observations in the WM (Hametner et al., 2013) and the previous cross-sectional imaging findings (Hernández-Torres et al., 2019), or stability in iron load, but not an increase in iron load.

2 | MATERIALS AND METHODS

2.1 | Subjects

In the present study, we included the same cohort of 160 participants, as in our recently published 2-year study (Hagemeier et al., 2018). In short, the study consisted of 120 MS patients (relapsing–remitting [RRMS]: 98, secondary-progressive [SPMS]: 22) and 40 age- and sex-matched normal controls (NC). Details about the inclusion and exclusion criteria are reproduced in Supplement 1. The study was approved by the local Ethical Standards Committee, and written informed consent was obtained from all participants.

2.2 | Image acquisition

We used the same MRI data as in the previous 2-year study. In brief, participants were imaged at both baseline and follow-up using the same 3 T GE Signa Excite HD 12.0 scanner (General Electric, Milwaukee, WI) with an eight-channel head-and-neck coil. In addition to 3D T_1 -weighted and FLAIR imaging (see Hagemeier et al., 2018), data for QSM were acquired using an unaccelerated 3D single-echo spoiled gradient recalled echo sequence with first-order flow compensation in read and slice directions, a matrix of $512 \times 192 \times 64$ and a nominal resolution of $0.5 \times 1 \times 2 \text{ mm}^3$ (FOV = $256 \times 192 \times 128 \text{ mm}^3$), flip angle = 12° , TE/TR = 22 ms/40 ms, bandwidth = 13.89 kHz, acquisition time = 8:46 minutes:seconds.

2.3 | Image analysis

2.3.1 | Segmentation, volumetry, QSM, and iron concentrations

Methods employed for segmentation and volumetry were described previously (Hagemeier et al., 2018). Specifically, as common in the literature, we normalized volumes with respect to subject head size for the *volumetry analysis*, referred to as *normalized volumes* in the following. For iron content analyses (see below) we used the nonnormalized raw volumes. We used the same reconstructed susceptibility maps and conversion to iron concentrations as in our previous study (Hagemeier et al., 2018). Briefly, the formula for conversion from susceptibility to iron concentration was calibrated through linear regression of susceptibility values measured in the HC group to histochemical iron values reported in the literature (Hallgren & Sourander, 1958). Different from previous studies, we obtained iron mass concentrations in mg iron per ml (volume), omitting the conversion from mass concentration to mass fractions in mg per 100 g tissue wet weight (100 g-ww). Iron mass concentrations can be used directly in the iron content estimation outlined in the next section. Details are reproduced in Supplement 1.

2.3.2 | Iron content

The total iron mass m_{Fe} (in mg) found in an anatomical region may be calculated by a voxel-wise integration of the local iron mass concentration over the volume of the structure of interest (Hernández-Torres et al., 2019):

$$m_{\text{Fe}} = \iiint_{\Omega} c_{\text{Fe}}(\vec{r}) dV$$

where $c_{\text{Fe}}(\vec{r})$ is the spatial distribution of the iron concentration, and Ω denotes the anatomical region. A simple way to execute the integration is by calculating the product of a region's average iron concentration $\langle c_{\text{Fe}} \rangle$ (in mg/ml) with the nonnormalized, raw volume V of the region (in ml): $m_{\text{Fe}} = \langle c_{\text{Fe}} \rangle \cdot V$. We calculated the iron content in the thalamus, caudate, putamen, and globus pallidus.

For the ease of readability, we will use the term *iron content* as a synonym for iron mass throughout the remainder of this article.

2.4 | Statistical analysis

Statistical analysis was conducted using SPSS (23.0, IBM, Armonk, NY) and R (3.2.1, R Foundation for Statistical Computing, Vienna, Austria). Outcome measures were averaged between both hemispheres, tested for normality using Q-Q plots and the Shapiro–Wilk test. It was assessed whether the variance between groups was

homogeneous using Levene's test and Box's M. As was done previously (Hagemeyer et al., 2018), mixed factorial ANOVA with an interaction term of time and group was used to investigate whether temporal trajectories of the dependent measures differed *between study groups*. Differences *between* study-groups at baseline and follow-up were tested using the Student's *t* test. Overtime effects *within* study-groups were tested using the paired *t* test. All analyses were repeated for RR- and SPMS sub-groups. Effect sizes were estimated using Hedges' *g*, and confidence intervals (CIs) refer to 95%.

Association analysis between magnetic susceptibility, volume, and iron content with age was explored using Pearson correlation coefficient within NCs. Within MS patients, associations of MRI measures with the change in Expanded Disability Status Scale (EDSS) and disease duration were investigated using age- and sex-adjusted regression models.

An α -level of 0.05 was set, with *p*-values adjusted for multiple comparisons using the false discovery rate method (*q*) below 0.05 being considered as statistically significant (Benjamini & Hochberg, 1995). Unadjusted *p* < 0.05 was considered as a trend.

3 | RESULTS

3.1 | Clinical, demographic, and MRI measures at baseline

The relationship between iron concentration, C_{Fe} , and magnetic susceptibility, χ , was determined as $C_{Fe} = \chi \cdot 0.147 \text{ mg/ml/ppb} + 4.885 \text{ mg/ml}$ (see Supplementary Material 1).

Supplement Table 1 lists baseline clinical, demographic, and MRI differences between controls and MS patients, identical to our previous study. No significant differences were observed between study groups concerning age, sex, and follow-up time. SP patients were older than RR patients (52.7 ± 6.7 vs. 42.0 ± 9.6 years; $p < 0.001$). The mean disease duration at baseline of the MS group was 12.8 ± 9.4 years. As expected, MS patients had higher T_2 -lesion volume and lower whole brain, gray matter, WM, and ventricular volumes compared to controls ($q \leq 0.048$).

Table 1 and Supplement Figure 2a summarize the calculated values of iron content in each DGM region studied cross-sectionally for NCs and MS patients. The highest iron content was observed in

TABLE 1 Baseline and follow-up regional iron content in patients and controls

| | | Baseline | Follow-up | <i>g</i> | Difference (95% CI) | % Change ^a (95% CI) |
|-----------------|--------------------------------|-----------------------------------|-----------------------------------|----------|----------------------------------|--------------------------------|
| Thalamus | Controls | 75.5 ± 18.8 | 76.0 ± 17.9 | .03 | +0.5 [−2.8, 3.7] | +0.7% [−3.7, 4.9] |
| | Multiple sclerosis | 55.7 ± 19.7 | 52.9 ± 18.1 | .15 | −2.8 [−4.7, −0.9] ^b | −5.0% [−8.4, −1.6] |
| | <i>g</i> | 1.02 | 1.28 | | | |
| | Difference (95% CI) | −19.8 (−26.8, −12.8) ^b | −23.1 (−26.8, −16.6) ^b | | | |
| | % Change ^a (95% CI) | −26.2% [−35.5, −16.9] | −30.4% [−35.3, −21.8] | | | |
| Caudate | Controls | 69.3 ± 12.0 | 70.9 ± 11.8 | .13 | +1.6 [−0.8, 4.1] | +2.3% [−1.2, 5.9] |
| | Multiple sclerosis | 71.7 ± 12.3 | 70.0 ± 13.2 | .14 | −1.7 [−2.8, −0.7] ^{b,c} | −2.4% [−3.9, −1.0] |
| | <i>g</i> | .20 | .07 | | | |
| | Difference (95% CI) | +2.4 (−2.4, 7.3) | −0.9 (−6.2, 3.2) | | | |
| | % Change ^a (95% CI) | +3.5% [−3.5, 10.5] | −1.3% [−8.7, 4.5] | | | |
| Putamen | Controls | 116.2 ± 21.4 | 115.7 ± 22.3 | .02 | −0.5 [−2.8, 1.7] | +0.4% [−2.4, 1.5] |
| | Multiple sclerosis | 112.0 ± 23.4 | 109.8 ± 24.6 | .09 | −2.2 [−3.8, −0.6] ^b | −2.0% [−3.4, 0.5] |
| | <i>g</i> | .18 | .05 | | | |
| | Difference (95% CI) | −4.2 (−12.4, 4.1) | −5.9 (−14.5, 2.8) | | | |
| | % Change ^a (95% CI) | −3.6% [−10.7, 3.5] | −5.1% [−12.5, 2.4] | | | |
| Globus pallidus | Controls | 70.3 ± 10.5 | 69.1 ± 9.3 | .12 | −1.2 [−2.9, 0.6] | −1.7% [−4.1, 0.9] |
| | Multiple sclerosis | 73.7 ± 17.4 | 71.1 ± 17.0 | .15 | −2.6 [−3.7, −1.4] ^b | −3.5% [−5.0, −1.9] |
| | <i>g</i> | .12 | .15 | | | |
| | Difference (95% CI) | +3.4 (−2.4, 9.1) | +2.0 (−3.6, 7.6) | | | |
| | % Change ^a (95% CI) | +4.8% [−3.4, 12.9] | +2.9% [−5.2, 11.0] | | | |

Note: Results are presented as mean ± standard deviation and mean difference (95% CI), respectively. Iron content is stated in mg. Effect sizes were computed using Hedge's *g*.

Abbreviation: CI, confidence interval.

^aPercent difference corresponding to the mean change and 95% lower and upper bounds.

^bSignificance after adjusting for false discovery rate at an alpha of $q < 0.05$.

^c $q < 0.05$ interaction effect of time by disease.

the putamen with up to 50% lower iron content in all other regions. The greatest cross-sectional group differences were observed in the thalamus, where a significantly lower iron content was observed in patients compared to NCs at both baseline and follow-up (−26.2 and −30.4%, respectively; $g \geq 1.02$; $q < 0.001$). No statistically significant cross-sectional group differences in iron content were observed in the caudate, putamen, and globus pallidus. A detailed description of the cross-sectional findings of iron content is provided in Supplement 2.

3.2 | Intra-subject temporal evolution

In NCs, the content of iron remained relatively stable in thalamus and putamen over 2 years (0.4–0.7%; $p > 0.633$; $g \leq 0.03$; Table 1 and Figure 2a), whereas effect sizes were higher in caudate ($g = 0.13$; +2.3%) and globus pallidus ($g = 0.12$; −1.7%). Changes over time did not reach significance ($p \geq 0.185$). In contrast, MS patients demonstrated significantly *decreasing* iron content over time in all regions (−2.0 to −5.0%; $g \geq 0.09$; $q \leq 0.014$). The difference in the evolution of iron content over 2 years *between* NC (+2.3%) and MS (−2.4%) (1.6 mg increase in NC, 1.7 mg decrease in MS) reached statistical significance in the caudate (interaction $F(1, 58) = 8.17$, $q = 0.009$).

Concerning the patient subgroups, we found a decrease over time in iron content in the thalamus (−3.2%, $q = 0.016$) as well as the caudate (−1.8%, $q = 0.016$) of patients with RRMS. The effect size of the iron content decline was similar in the caudate of patients with SPMS, but the change over time did not reach statistical significance, likely due to the smaller group size. In the thalamus of SPMS patients, the effect size of declining iron content was only 30% of that in RRMS patients ($g = 0.18$ vs. 0.05), suggesting that thalamic iron content remained relatively stable over 2 years in progressive patients ($p = 0.602$; Table 2 and Figure 2b). In contrast, both RRMS and SPMS patients showed decreasing iron content over time in the caudate and putamen, with SPMS showing the strongest iron content reductions (putamen: RRMS: −2.0% SPMS: −3.2%; $p < 0.05$, globus pallidus: RRMS: −2.0%, SPMS: −4.7%; $q \leq 0.016$).

Caudate and thalamus demonstrated a 40% (−2.5 vs. −1.8%) and 175% (−5.5 vs. −2.0%) faster pace in iron content decline in RRMS patients than in SPMS patients over the 2 years, respectively. In putamen and globus pallidus, we observed the opposite pattern with a 55% (−1.8 vs. −2.8%) and 125% (−2.7 vs. −6.1%) faster pace of decline in SPMS patients than in RRMS patients, respectively. However, interaction terms did not reach statistical significance.

3.3 | Association of iron content with demographic and clinical outcomes

In NCs, volumes of thalamus ($r = -0.487$, $q = 0.001$) and caudate ($r = -0.475$, $q = 0.017$) and susceptibility in the caudate ($r = 0.494$, $q = 0.001$) and putamen ($r = 0.545$, $q < 0.001$) correlated significantly with age. We did not find a significant correlation of iron content with age, suggesting that age-specific effects of change in iron are mediated primarily by atrophy.

In age- and sex-adjusted regression models (Supplement Table 3), patients with higher disease duration were found to have a lower *baseline* iron content in the putamen, caudate, and thalamus ($\beta \leq -0.302$, $p \leq 0.002$), but not in globus pallidus ($p = 0.12$). Similar associations with disease duration were seen for iron concentration only in the putamen ($\beta = -0.236$, $p = 0.032$) and for volumes only in the thalamus ($\beta = -0.379$, $p = 0.001$).

Of all *baseline* MRI metrics (Supplement Table 3), we found associations with *baseline* EDSS ($\beta \leq -0.203$) only for normalized volumes (thalamus, globus pallidus; $p \leq 0.027$), but neither for iron concentrations nor iron content ($p > 0.06$). However, *disability progression over 2 years* was associated with lower *baseline* volumes of the caudate and putamen ($\beta = -0.185$, $p \leq 0.046$), but not of thalamus and globus pallidus ($p > 0.26$). On the contrary, *disability progression over 2 years* was associated with neither *baseline* iron concentration nor *baseline* iron content in caudate and putamen ($p > 0.37$), but with both *lower baseline* iron concentration and *lower baseline* iron content in the thalamus ($\beta \leq -0.197$, $p \leq 0.025$), as well as to *higher baseline* iron concentration in the pallidum ($\beta = 0.208$, $p = 0.027$).

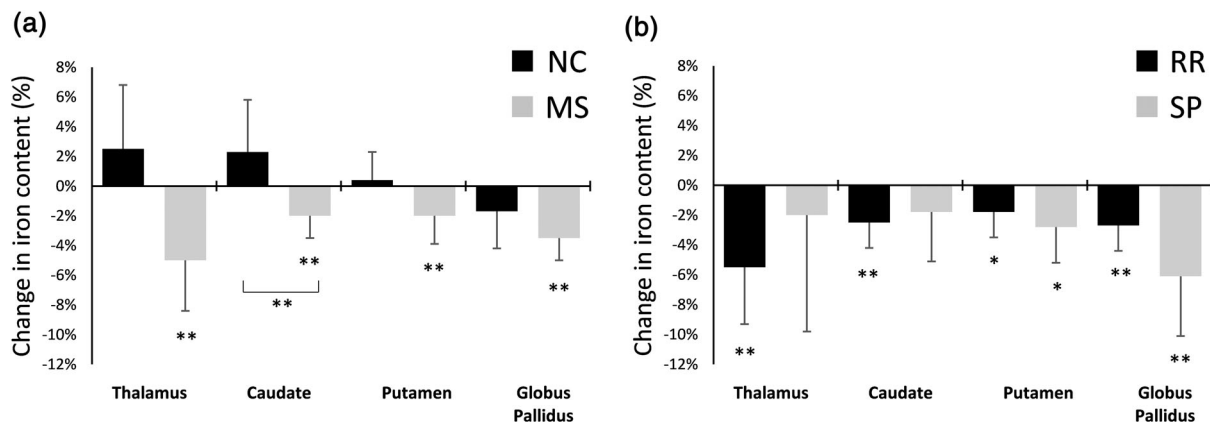


FIGURE 2 Percent change of regional iron content relative to baseline iron content over 2 years for (a) multiple sclerosis patients (multiple sclerosis [MS]; gray) and normal controls (normal control [NC]; black), and (b) relapsing-remitting (RR) MS (black) and secondary progressive (SP) MS (gray) patients. *Unadjusted $p < 0.05$. **False discovery rate adjusted $q < 0.05$. Brackets refer to an interaction effect of the groups over 2 years at $q < 0.05$. Error bars represent the 95% confidence interval of the change

TABLE 2 Baseline and follow-up regional iron content in RR and SP MS patients

| | | Baseline | Follow-up | <i>g</i> | Difference (95% CI) | % Change ^a (95% CI) |
|-----------------|--------------------------------|----------------------------------|---------------------------------|----------|--------------------------------|--------------------------------|
| Thalamus | Relapsing | 58.2 ± 18.9 | 55.0 ± 17.6 | .18 | -3.2 (-5.5, -1.1) ^b | -5.5% (-9.5, -1.9) |
| | Progressive | 44.4 ± 19.6 | 43.5 ± 17.6 | .05 | -0.9 (-4.5, 2.7) | -2.0% (-10.1, 6.1) |
| | <i>g</i> | .71 | .65 | | | |
| | Difference (95% CI) | -13.8 (-22.7, -4.9) ^b | -11.5 (-19.7, 3.2) ^b | | | |
| | % Change ^a (95% CI) | -23.7% (-39.0, -8.4) | -20.9% (-35.8, -5.8) | | | |
| Caudate | Relapsing | 71.5 ± 14.1 | 69.7 ± 13.7 | .13 | -1.8 (-3.1, -0.6) ^b | -2.5% (-4.3, -0.8) |
| | Progressive | 72.6 ± 11.1 | 71.3 ± 10.8 | .12 | -1.3 (-3.7, 1.1) | -1.8% (-5.1, 1.5) |
| | <i>g</i> | .09 | .13 | | | |
| | Difference (95% CI) | +1.1 (-5.3, 7.4) | +1.6 (-4.6, 7.8) | | | |
| | % Change ^a (95% CI) | +1.5% (-7.4, 10.3) | +2.3% (-6.6, 11.2) | | | |
| Putamen | Relapsing | 111.4 ± 22.9 | 109.4 ± 23.9 | .09 | -2.0 (-3.8, -0.1) ^c | -1.8% (-3.4, -0.1) |
| | Progressive | 115.0 ± 25.8 | 111.8 ± 28.1 | .12 | -3.2 (-6.0, -0.4) ^c | -2.8% (-5.2, -0.3) |
| | <i>g</i> | .02 | .09 | | | |
| | Difference (95% CI) | +3.6 (-8.6, 15.9) | +2.4 (-9.1, 14.0) | | | |
| | % Change ^a (95% CI) | +3.2% (-7.7, 14.2) | +2.2% (-8.3, 12.8) | | | |
| Globus pallidus | Relapsing | 73.0 ± 16.7 | 71.0 ± 16.5 | .12 | -2.0 (-3.3, -0.8) ^b | -2.7% (-4.5, -1.1) |
| | Progressive | 76.6 ± 20.4 | 71.9 ± 19.8 | .23 | -4.7 (-7.8, -1.7) ^b | -6.1% (-10.2, -2.2) |
| | <i>g</i> | .19 | .05 | | | |
| | Difference (95% CI) | +3.6 (-4.5, 11.8) | +0.9 (-7.1, 8.9) | | | |
| | % Change ^a (95% CI) | +4.9% (-6.1, 16.2) | +1.3% (-10.0, 12.5) | | | |

Note: Results are presented as mean ± SD and mean difference (95%), respectively. Iron content is stated in mg. Effect sizes were computed using Hedge's *g*. No interaction effect of time by disease ($q < 0.05$) was observed.

Abbreviations: CI, confidence interval; RR, relapsing-remitting; SP, secondary progressive.

^aPercent difference corresponding to the mean change and 95% lower and upper bounds.

^bSignificance after adjusting for false discovery rate at an alpha of $q < 0.05$.

^cSignificance at an unadjusted (trend level) alpha of $p < .05$.

Among all changes in MRI metrics over 2 years (Supplement Table 4), we found only an association between disability progression and declining thalamic volumes ($\beta = -0.209$, $p = 0.032$). Changes over 2 years in neither iron content nor iron concentration were significantly associated with EDSS measures or disease duration ($p > 0.077$), potentially due to the short time-frame of the follow-up.

Baseline iron content in patients was also associated with T_2 (thalamus: $\beta = -0.440$, $q < 0.001$, putamen: $\beta = -0.237$, $q = 0.018$) and T_1 -lesion volumes (thalamus: $\beta = -0.295$, $q = 0.004$; caudate: $\beta = -0.216$, $q = 0.022$; putamen: $\beta = -0.272$, $p = 0.008$). Change in iron content was associated with percent whole-brain volume change (caudate: $\beta = 0.231$, $p = 0.018$), suggesting that decreasing iron content is associated with global disease-related neurodegeneration.

4 | DISCUSSION

In our previous work, using identical imaging data as in the present study, we reported increasing iron concentrations over 2 years in patients, and in patients compared to NCs (Hagemeyer et al., 2018). The present study investigated alterations in DGM tissue iron content by combining the magnetic tissue susceptibility with structural

volume. Supplement Table 2 compares the findings of the present study with those in our previous study. In the following, we will discuss the biological relevance of these findings in light of the vast body of literature that inferred on iron homeostasis using (raw) iron concentration measurements.

4.1 | Biological relevance of increasing iron concentration

As discussed above, iron concentration can increase due to pathological processes that do neither affect the iron load nor the number of iron-containing cells. Consequently, the biological relevance of increased iron concentrations, as observed with iron-MRI, is unclear. It is highly unlikely that the mere increase in density of otherwise healthy iron-containing cells in such a scenario would give rise to oxidative stress. Fenton chemistry requires free iron, and a consensus exists that safely stored and regulated iron in ferritin complexes does not promote oxidative stress.

Strong synaptophysin staining, which is similar in MS and control cases (Vercellino et al., 2009) and a relatively low density of cell bodies, that is, cellularity, on H&E stains (Haider et al., 2014) suggest that

the DGM volume is dominated by neuropil, similar to the neocortex. Structural atrophy is likely linked to an absolute volume loss in this neuropil and nerve cells (Cifelli et al., 2002). Compared to glia cells, which stain strongly but sparsely in the DGM, neuropil and nerve cells contain low iron concentrations (Haider et al., 2014). Consequently, a loss in neuropil and nerve cells, which together store only little amounts of iron, can result in increased regional iron concentrations. The interpretation of increased iron concentrations obtained with QSM is further complicated in the presence of demyelination. Since myelin is diamagnetic, demyelination can increase the local susceptibility and, thus, mimic increased iron concentration. Histopathology has shown a high abundance of demyelinating lesions in the DGM (Haider et al., 2014), raising the question if previous reports of increased iron concentrations were also driven at least in part by demyelination. This consideration, however, does not apply to previous findings of increased R_2^* values because demyelination has an opposed effect on R_2^* values.

4.2 | Previous studies

Most previous iron-MRI studies relied on (raw) measures of iron concentration. While some of these studies adjusted for volume differences by using volume as a statistical covariate, this approach merely determines if variations in iron concentrations are independent of variations in volumes. Controlling for volume does not provide direct insights on alterations in the regional iron content.

An exception is the recent study by Hernández-Torres et al. (2019) that estimated iron content *cross-sectionally* using R_2^* instead of QSM. While iron concentrations were increased in MS patients (caudate and globus pallidus), the authors reported reduced (thalamus, caudate) or similar (putamen, globus pallidus) iron content in MS patients compared to NC. These findings are consistent with our cross-sectional results, which we discussed in Supplement 2. However, although the myelin content is low in most DGM regions to begin with, demyelination has an opposite effect on R_2^* compared to QSM and findings in the study by Hernández-Torres et al. may have been driven by a loss in myelin rather than by a loss in iron. Elkady, Cobzas, Sun, Blevins, and Wilman (2018) and Elkady et al. (2019) addressed this issue by combining QSM and R_2^* in two more recent longitudinal studies over 2 ($N = 44$ patients) and 5 years ($N = 25$). These two studies confirmed previous findings and provided further support for decreasing thalamic iron content.

4.3 | Biological relevance of decreasing iron content

The majority of brain iron is found in oligodendrocytes (Bagnato et al., 2011; Francois, Nguyen-Legros, & Percheron, 1981; Haider et al., 2014; Hametner et al., 2013; Hill & Switzer III, 1984; Meguro, Asano, Odagiri, Li, & Shoumura, 2008), where it is primarily localized in mitochondria and used for the production and consumption of

adenosine triphosphate (Fiorito, Chiabrando, & Tolosano, 2018; Lane et al., 2015; Paul, Manz, Torti, & Torti, 2017). Hence, regional iron content may be considered as a marker of the *total amount* of iron that is available for the metabolic function of the oligodendrocyte ensemble in the region.

In the present study, MS patients displayed a decline in overall iron content in all regions, with the most robust effect sizes in the thalamus (MS: $g = 0.15$, RR: $g = 0.18$) and globus pallidus (MS: $g = 0.15$, SP: $g = 0.23$). In our schematic tissue model, reduced iron content can be caused by a reduction in the number of iron-containing cells (Figure 1b–d), an efflux of iron from iron-laden cells followed by clearance from the region, or both (Table 3). Such scenarios are consistent with histopathological findings in MS by Hametner et al. (2013), albeit in the WM. The authors reported a reduction of iron and an upregulation of iron exporting ferroxidases in oligodendrocytes.

While oligodendrocytes in the GM show an even higher iron content (Haider et al., 2014) than their myelinating siblings in the WM (Baumann & Pham-Dinh, 2001; Simons & Nave, 2016), knowledge about their specific function in the GM is still limited (Verkhatsky, 2013). Recent studies indicate that GM oligodendrocytes regulate neuronal activity (Battfeld, Klooster, & Kole, 2016) and bear essential roles in the trophic maintenance of projecting neurons (Takasaki et al., 2010). Our results suggest a reduction in the oligodendroglial iron availability, which may be linked to neurodegeneration and impairment through these proposed mechanisms.

4.4 | Biological relevance of simultaneously increasing (or stable) iron concentration and decreasing iron content

In our previous study, iron concentrations were relatively stable in thalamus and globus pallidus over the 2 years, whereas caudate and putaminal concentrations increased between 3 and 9%. The present study illustrated that these findings are associated with a simultaneous reduction in iron content.

Alterations in region-average iron concentration and iron content provide complementary insights on the underlying biology (Figure 1). Table 3 lists expected changes in iron concentration and iron content for different pathological scenarios. Only three of the fifteen scenarios lead to increasing concentration and simultaneously decreasing content of iron (as seen in caudate and putamen): (a) a rapid loss of iron-free cells with a mild iron efflux from iron-containing cells; (b) a similar loss in both iron-containing and iron-free cells with a small amount of iron influx; (c) loss in iron-free cells occurs more rapidly than the loss in iron-containing cells (no influx or efflux of iron). Another three of the scenarios lead to stable iron concentration with decreasing iron content (as seen in thalamus and globus pallidus): (d) similar loss of iron-free and iron-containing cells without iron influx; (e) moderate iron efflux with significantly faster loss in iron-free than iron-containing cells; and (f) moderate iron efflux with loss of iron-free but not iron-containing cells.

TABLE 3 Expected alterations in iron concentration (c_{Fe}) and content (m_{Fe}) resulting from tissue atrophy in different pathological scenarios: (i) no iron influx into the region; (ii) iron influx into the region occurred; and (iii) iron is removed from iron-containing cells. The asterisk * highlights the four scenarios in which iron-containing cells are *not* affected by the pathological processes. The conclusion is that declining iron content always implies the involvement of iron-containing cells, either through a reduction in their number or a loss of intracellular iron. A simultaneous decline in iron content and iron concentration always implies a reduction in the number of iron-containing cells, potentially with a mild influx of iron into the region. Simultaneously declining iron content and increasing iron concentration can be caused by a mild loss in cellular iron, even without a reduction in the number of iron-containing cells or a mild reduction in the number of iron-containing cells, potentially with a mild iron influx

| Change in the number of cells | | Scenario | | | | | |
|-------------------------------|-----------------|----------------|----------|--------------------------|----------|--------------------|----------|
| | | No iron influx | | Iron influx ^a | | Cellular iron loss | |
| Iron-containing cells | Iron-free cells | c_{Fe} | m_{Fe} | c_{Fe} | m_{Fe} | c_{Fe} | m_{Fe} |
| ---- | | ↓ | ↓ | ↓↔↑ | ↓↔↑ | ↓ | ↓ |
| ---- | - | | | | | | |
| -- | -- | ↔ | ↓ | ↑ | ↓↔↑ | ↓ | ↓ |
| - | ---- | ↑ | ↓ | ↑ | ↓↔↑ | ↑↔↓ | ↓ |
| | ---- | ↑* | ↔* | ↑* | ↑* | ↑↔↓ | ↓ |

Note: ↑: increased values; ↓: decreased values; ↔: no change in values. ↓↔↑ or ↑↔↓: change in values depends on the relative pace of iron influx/loss compared to the regional volume loss. ↓↔↑: indicates that values will decrease if the amount of iron flowing into the region is too small to compensate for the loss of iron from a reduction in the number of iron-containing cells, values will remain constant if iron influx exactly compensates for the iron loss resulting from a decline in iron-containing cells. Values will increase if enough iron is flowing in to overcompensate the loss in iron-containing cells. ↑↔↓: indicates that values will increase if the amount of iron released from cells is too small to compensate for the increase in iron concentration due to a loss in iron-free cells, values will remain constant if iron loss exactly compensates for the volume decline. Values will decrease if enough iron is removed from cells to overcompensate the volume decline.

^aSince both demyelination and iron increase the magnetic susceptibility, the column "iron influx" also reflects the potential effect of confounding contributions from demyelination on the calculated values of c_{Fe} and m_{Fe} .

At this point, we would like to stress that neither iron content nor iron concentration, as measured with QSM, would be affected by a transfer of iron *between* cells *within* the region. Such a transfer occurs, for example, if cellular debris is taken up by surrounding cells (microglia, macrophages) following cell death (Hametner et al., 2013). The net regional iron content or concentration is only affected if the iron is physically cleared from the region. Iron transfer may be studied in vivo with a recently proposed technique that combines R_2^* (which is sensitive to cellular iron load) and QSM, and preliminary data suggests that it can be observed in MS patients (Taage et al., 2019).

Neurodegeneration is often followed by secondary demyelination or it is a consequence of primary demyelination itself. Both phenomena are likely linked also to a change in the oligodendrocyte number. Such a causal interrelationship would result in stable iron concentrations, along the lines of scenario (d).

While we cannot conclude whether iron efflux from or a loss in the number of iron-containing cells (or both) occurred in our sample, our results suggest that iron-containing cells are involved in or affected by pathology in all studied regions. Our theoretical considerations suggest that this phenomenon may be studied in vivo through the iron content metric.

4.5 | Dynamics of changes in iron content throughout the disease

The decline in iron content over 2 years occurred more rapidly in the thalamus (−5.5%) and caudate (−2.5%) of RRMS patients than of

SPMS patients (−2.0 and −1.8%, respectively). We saw the opposite pattern in the putamen (−1.8 vs. −2.8%) and globus pallidus (−2.7 vs. −6.1%), where iron content decreased more rapidly in SPMS patients than RRMS patients. These observations suggest that oligodendroglia in the thalamus and caudate are affected early in the disease, whereas putaminal and pallidal oligodendrocytes are affected in later phases. While an early involvement of the thalamus is consistent with previous studies (Eshaghi et al., 2018; Henry et al., 2008; Henry et al., 2009; Zivadivov et al., 2013), our results are only a snapshot of 2 years in our specific cohort, and more extended longitudinal studies at various stages of the disease need to confirm and further elucidate these dynamics.

4.6 | Clinical relevance of iron content compared to other imaging markers

Our findings suggest that iron content is a more robust imaging marker of MS disease progression than either volume or iron concentration alone. First, this finding is striking since iron content comprises uncorrelated noise from the individual measurements of volume and iron. Hence, iron content would be expected to be noisier than each of the original measures. While the effect sizes of overtime changes in iron content were smaller than those of volumes in most regions of patients (Hagemeyer et al., 2018), they were higher than those of iron concentrations in all regions. Second, iron *content* in several DGM nuclei was more strongly associated with disease duration than either normalized structural volumes or iron concentrations (Supplement

Table 3, independent of age). Third, in the thalamus, lower iron content was associated with disability worsening *over time*, albeit with a slightly smaller absolute effect size than the iron concentration ($\beta = -.197$ vs. $-.257$), but not with baseline disability. On the contrary, thalamic volume was associated with baseline disability, but not with a change in disability over time. Taken together, it appears that the benefit of combining the two metrics outweighs the increased noise level.

Finally, iron content was relatively age-independent, whereas both iron concentration and structural volumes were dependent on age. Independence of age renders iron content particularly beneficial for assessing disease-specific tissue alterations because it does not require accounting for atrophy or alterations in iron concentration associated with aging. Overall, our findings indicate that iron content holds promise as a contributor to a future composite imaging biomarker of disease progression in clinical trials.

4.7 | Study limitations

Our work has several limitations. First, our study involved only two time points, which prevented examining the lead-lag relations between volume, iron concentration, and iron content. In a multi time-point study, Daugherty and Raz (2016) showed that increased iron concentration preceded shrinkage in the putamen of healthy subjects. A similar study design with iron content would provide essential insights into the temporal dynamics between iron concentrations, iron content, and neurodegeneration.

Second, our study did not involve a marker of myelin content. Demyelination can mimic *increased* iron concentration and iron content. Histopathology by Haider et al. showed that demyelination and iron loss are collocated in lesions of the DGM (Haider et al., 2014). The authors reported that in half of the included specimens from patients with RRMS, more than 40% of the caudate nucleus area was demyelinated, compared to only 6% of the thalamus and even less of globus pallidus and putamen (Figure 1a therein). Based on these previous findings, we would have expected the most considerable change in iron content in caudate and much smaller effects in the other regions. Contrarily, we found the most considerable alterations in the thalamus, and much smaller alterations in all other regions, including the caudate. This discrepancy may partially be explained by the opposing effect of demyelination on the estimated iron content compared to iron loss: The loss of diamagnetic myelin systematically increases QSM-based iron content estimations, implying that demyelination and iron loss may (partially) cancel out one another. As such, demyelination has likely *reduced* effect sizes in the present study. Future studies may explore the inclusion of myelin-specific metrics in the iron content calculation to yield even higher sensitivity, but need to consider that myelin metrics are confounded by tissue alterations seen in MS, such as inflammation and alterations in iron concentrations (Birkel et al., 2019; Gareau, Rutt, Karlik, & Mitchell, 2000; Vavassour, Laule, Li, Traboulsee, & MacKay, 2011).

Third, along the lines of the potential effect of demyelination, remyelination may also have had a biasing effect on our study. Opposite to demyelination, remyelination can mimic a *decrease* in iron concentration and iron content *over time*. We observed a significant decline in T₂-lesion volumes in patients over the 2 years (-0.54 ± 1.39 ml; $p = 0.02$), which could be due to remyelination activity in our sample. Another explanation for this finding would be the recently reported replacement of T₂-lesions by cerebrospinal fluid spaces (Dwyer et al., 2018; Genovese et al., 2019).

Fourth, it is known that T₁-based segmentation techniques can suffer from inaccuracies in regions where T₁-contrast is limited. Furthermore, Lorio et al. (2014) have shown that the use of probability map integrals or voxel-wise comparisons as a surrogate for real volume in intensity-probability-based morphological analyses can lead to biased structural volume estimations depending on the iron concentration. In the present work, we used a state-of-the-art constrained shape-fitting approach (FSL FIRST (Patenaude, Smith, Kennedy, & Jenkinson, 2011)), which is theoretically much less sensitive to these kinds of biases. In comparison with similar algorithms for DGM segmentation, FIRST has produced the most accurate segmentation in patients with MS (Derakhshan et al., 2010). However, due to the declining T₁ contrast with increasing iron concentrations, it is possible that volumes have been systematically underestimated in regions with higher iron concentration, representing a potential source of bias toward reduced iron content in patients. However, our findings in the present study were largely in-line with the cross-sectional study by Hernández-Torres et al. (2019) that used a manual region-tracing approach. Hence, while the effect size of iron content decline may have been overestimated, it is unlikely that our primary findings of decreased iron content were driven by segmentation artifacts.

We also did not observe the high rate of failure of FIRST that was reported by Hernández-Torres et al. (2019), probably due to differences in parameters of the T₁-weighted pulse sequence. However, it has also been shown that FSL FIRST can result in inaccurate segmentations when brains are severely atrophied (Feng et al., 2017), especially in the globus pallidus. While this issue may have biased our between-group comparisons, a relevant effect on the overtime analyses is less likely. The present study used FIRST primarily to enable the direct side-by-side comparison of iron content with iron concentration reported in our previous study, which had used this same technique. More sophisticated atlas-based techniques (Li et al., 2019; Schweser et al., 2018) may reduce variance and increase effect sizes in future studies.

4.8 | Conclusion

In summary, our study suggests that the widely reported observation of increased DGM iron concentrations in MS patients is at least partially *driven* by a loss in cells with little or no iron. Our findings shed new light on the vast body of imaging research that has been the primary supporting evidence for the notion that neurodegeneration in

MS is linked to an influx of iron into the DGM. Until additional evidence exists, we recommend that differences in regional tissue iron concentrations are only interpreted in a proper context of alterations in the structural volume, such as in tandem with an iron-content metric. In this study, iron content in several DGM regions was more robustly linked to disease duration than iron concentrations or structural volumes, and thalamic iron content predicted disability worsening more robustly than DGM volumes in any of the regions.

ACKNOWLEDGMENTS

The research reported in this publication was funded by the National Center for Advancing Translational Sciences of the National Institutes of Health under Award Number UL1TR001412. The content is solely the responsibility of the authors and does not necessarily represent the official views of the NIH.

CONFLICT OF INTEREST

J. H., S. H., and N. B. have nothing to disclose. M. G. D. has received consultant fees from Claret Medical and EMD Serono, and research support from Novartis and Celgene. B. W.-G. has participated in speaker's bureaus and/or served as a consultant for Biogen, Novartis, Genzyme and Sanofi, Genentech, Abbvie, Bayer AG, and Celgene/BMS. Dr B. W.-G. also has received grant/research support from the agencies listed in the previous sentence as well as Mallinckrodt Pharmaceuticals, Inc. She serves in the editorial board for *BMJ Neurology*, *Journal of International MS*, *CNS Drugs*, *Children and Frontiers of Epidemiology*. R. Z. received personal compensation from EMD Serono, Sanofi, Bristol Myers Squibb, and Novartis for speaking and consultant fees. He received financial support for research activities from Mapi Pharma, Bristol Myers Squibb, Novartis, Protekto, Keystone Heart, V-WAVE Medical and Boston Scientific. F. S. received personal compensation from Toshiba Canada Medical Systems Limited, Canon Medical Systems Corporation Japan, and Goodwin Procter LLP for speaking and consultant fees. He received financial support for research activities from SynchroPET Inc. and travel sponsorship from GE Healthcare and SynchroPET Inc.

AUTHOR CONTRIBUTIONS

Ferdinand Schweser: Conceptualization, funding acquisition, methodology, project administration, resources, software, supervision, validation, visualization, writing—original draft. **Jesper Hagemeyer:** Data curation, formal analysis, methodology, visualization, writing—original draft. **Niels Bergsland** and **Mike Dwyer:** Formal analysis, software, writing—review and editing. **Simon Hametner:** Writing—review and editing. **Bianca Weinstock-Guttman:** Resources, writing—review and editing. **Robert Zivadinov:** Funding acquisition, resources, writing—review and editing.

DATA AVAILABILITY STATEMENT

The data that support the findings of this study are available on a reasonable request to the corresponding author (F. S.). The data are not publicly available due to containing information that could compromise the privacy of research participants.

ORCID

Ferdinand Schweser  <https://orcid.org/0000-0003-0399-9211>
 Jesper Hagemeyer  <https://orcid.org/0000-0002-3286-5207>
 Michael G Dwyer  <https://orcid.org/0000-0003-4684-4658>
 Niels Bergsland  <https://orcid.org/0000-0002-7792-0433>

REFERENCES

- Bagnato, F., Hametner, S., Yao, B., van Gelderen, P., Merkle, H., Cantor, F. K., ... Duyn, J. H. (2011). Tracking iron in multiple sclerosis: A combined imaging and histopathological study at 7 tesla. *Brain*, *134*, 3599–3612.
- Battefeld, A., Klooster, J., & Kole, M. H. P. (2016). Myelinating satellite oligodendrocytes are integrated in a glial syncytium constraining neuronal high-frequency activity. *Nature Communications*, *7*, 1–13.
- Baumann, N., & Pham-Dinh, D. (2001). Biology of oligodendrocyte and myelin in the mammalian central nervous system. *Physiological Reviews*, *81*, 871–927.
- Benjamini, Y., & Hochberg, Y. (1995). Controlling the false discovery rate: A practical and powerful approach to multiple testing. *Journal of the Royal Statistical Society Series B*, *57*, 289–300.
- Bergsland, N., Schweser, F., Dwyer, M. G., Weinstock-Guttman, B., Benedict, R. H. B., & Zivadinov, R. (2018). Thalamic white matter in multiple sclerosis: A combined diffusion-tensor imaging and quantitative susceptibility mapping study. *Human Brain Mapping*, *39*, 4007–4017.
- Bergsland, N., Tavazzi, E., Schweser, F., Jakimovski, D., Hagemeyer, J., Dwyer, M. G., & Zivadinov, R. (2019). Targeting iron dyshomeostasis for treatment of neurodegenerative disorders. *CNS Drugs*, *33*, 1073–1086.
- Bergsland, N. P., Horakova, D., Dwyer, M. G., Dolezal, O., Seidl, Z. K., Vaneckova, M., ... Zivadinov, R. (2012). Subcortical and cortical gray matter atrophy in a large sample of patients with clinically isolated syndrome and early relapsing-remitting multiple sclerosis. *American Journal of Neuroradiology*, *33*, 1573–1578.
- Bilgic, B., Pfefferbaum, A., Rohlfing, T., Sullivan, E. V., & Adalsteinsson, E. (2012). MRI estimates of brain iron concentration in normal aging using quantitative susceptibility mapping. *NeuroImage*, *59*, 2625–2635.
- Birkel, C., Birkel-Toegelhofer, A. M., Endmayr, V., Hoftberger, R., Kasprian, G., Krebs, C., ... Rauscher, A. (2019). The influence of brain iron on myelin water imaging. *NeuroImage*, *199*, 545–552. <https://doi.org/10.1016/j.neuroimage.2019.05.042>.
- Burgetova, A., Dusek, P., Vaneckova, M., Horakova, D., Langkammer, C., Krasensky, J., ... Seidl, Z. (2017). Thalamic iron differentiates primary-progressive and relapsing-remitting multiple sclerosis. *American Journal of Neuroradiology*, *38*, 1079–1086.
- Cifelli, A., Arridge, M., Jezzard, P., Esiri, M. M., Palace, J., & Matthews, P. M. (2002). Thalamic neurodegeneration in multiple sclerosis. *Annals of Neurology*, *52*, 650–653.
- Connor, J. R., Snyder, B. S., Arosio, P., Loeffler, D. A., & le Witt, P. (1995). A quantitative analysis of isoferritins in select regions of aged, Parkinsonian, and Alzheimer's diseased brains. *Journal of Neurochemistry*, *65*, 717–724.
- Craelius, W., Migdal, M. W., Luessenhop, C. P., Sugar, A., & Mihalakis, I. (1982). Iron deposits surrounding multiple sclerosis plaques. *Archives of Pathology & Laboratory Medicine*, *106*, 397–399.
- Daugherty, A. M., & Raz, N. (2016). Accumulation of iron in the putamen predicts its shrinkage in healthy older adults: A multi-occasion longitudinal study. *NeuroImage*, *128*, 11–20.
- Derakhshan, M., Caramanos, Z., Giacomini, P. S., Narayanan, S., Maranzano, J., Francis, S. J., ... Collins, D. L. (2010). Evaluation of automated techniques for the quantification of grey matter atrophy in patients with multiple sclerosis. *NeuroImage*, *52*, 1261–1267.

- Dwyer, M. G., Bergsland, N., Ramasamy, D. P., Jakimovski, D., Weinstock-Guttman, B., & Zivadinov, R. (2018). Atrophied brain lesion volume: A new imaging biomarker in multiple sclerosis: Atrophied lesions in MS. *Journal of Neuroimaging*, 28, 490–495.
- Elkady, A. M., Cobzas, D., Sun, H., Blevins, G., & Wilman, A. H. (2018). Discriminative analysis of regional evolution of iron and myelin/calcium in deep gray matter of multiple sclerosis and healthy subjects: Analysis of iron and myelin in MS. *Journal of Magnetic Resonance Imaging*, 48, 652–668.
- Elkady, A. M., Cobzas, D., Sun, H., Seres, P., Blevins, G., & Wilman, A. H. (2019). Five year iron changes in relapsing-remitting multiple sclerosis deep gray matter compared to healthy controls. *Multiple Sclerosis and Related Disorders*, 33, 107–115.
- Eshaghi, A., Prados, F., Brownlee, W., Altmann, D. R., Tur, C., Jorge Cardoso, M., ... Ciccarelli, O. (2018). Deep grey matter volume loss drives disability worsening in multiple sclerosis. *Annals of Neurology*, 83(2), 2–38. <https://doi.org/10.1002/ana.25145>.
- Feng, X., Deistung, A., Dwyer, M. G., Hagemeyer, J., Polak, P., Lebenberg, J., ... Schweser, F. (2017). An improved FSL-FIRST pipeline for subcortical gray matter segmentation to study abnormal brain anatomy using quantitative susceptibility mapping (QSM). *Magnetic Resonance Imaging*, 39, 110–122.
- Filippi, M., Bruck, W., Chard, D., Fazekas, F., Geurts, J. J. G., Enzinger, C., ... Lassmann, H. (2019). Association between pathological and MRI findings in multiple sclerosis. *Lancet Neurology*, 18, 198–210.
- Fiorito, V., Chiabrando, D., & Tolosano, E. (2018). Mitochondrial targeting in neurodegeneration: A heme perspective. *Pharmaceuticals*, 11, 87.
- Francois, C., Nguyen-Legros, J., & Percheron, G. (1981). Topographical and cytological localization of iron in rat and monkey brains. *Brain Research*, 215, 317–322.
- Gareau, P. J., Rutt, B. K., Karlik, S. J., & Mitchell, J. R. (2000). Magnetization transfer and multicomponent T2 relaxation measurements with histopathologic correlation in an experimental model of MS. *Journal of Magnetic Resonance Imaging*, 11(6), 586–595.
- Genovese, A. V., Hagemeyer, J., Bergsland, N., Jakimovski, D., Dwyer, M. G., Ramasamy, D. P., ... Zivadinov, R. (2019). Atrophied brain T2 lesion volume at MRI is associated with disability progression and conversion to secondary progressive multiple sclerosis. *Radiology*, 293, 424–433.
- Hagemeyer, J., Dwyer, M. G., Bergsland, N. P., Schweser, F., Magnano, C. R., Heininen-Brown, M., ... Zivadinov, R. (2013). Effect of age on MRI phase behavior in the subcortical deep gray matter of healthy individuals. *American Journal of Neuroradiology*, 34, 2144–2151.
- Hagemeyer, J., Geurts, J. J. G., & Zivadinov, R. (2012). Brain iron accumulation in aging and neurodegenerative disorders. *Expert Review of Neurotherapeutics*, 12, 1467–1480.
- Hagemeyer, J., Zivadinov, R., Dwyer, M. G., Polak, P., Bergsland, N., Weinstock-Guttman, B., ... Schweser, F. (2018). Changes of deep gray matter magnetic susceptibility over 2 years in multiple sclerosis and healthy control brain. *NeuroImage: Clinical*, 18, 1007–1016.
- Haider, L., Simeonidou, C., Steinberger, G., Hametner, S., Grigoriadis, N., Deretzi, G., ... Frischer, J. M. (2014). Multiple sclerosis deep grey matter: The relation between demyelination, neurodegeneration, inflammation and iron. *Journal of Neurology, Neurosurgery, and Psychiatry*, 85, 1386–1395.
- Hallgren, B., & Sourander, P. (1958). The effect of age on the non-haemin iron in the human brain. *Journal of Neurochemistry*, 3, 41–51.
- Hametner, S., Wimmer, I., Haider, L., Pfeifenbring, S., Brück, W., & Lassmann, H. (2013). Iron and neurodegeneration in the multiple sclerosis brain. *Annals of Neurology*, 74, 848–861.
- Henry, R. G., Shieh, M., Amirbekian, B., Chung, S., Okuda, D. T., & Pelletier, D. (2009). Connecting white matter injury and thalamic atrophy in clinically isolated syndromes. *Journal of the Neurological Sciences*, 282, 61–66.
- Henry, R. G., Shieh, M., Okuda, D. T., Evangelista, A., Gorno-Tempini, M. L., & Pelletier, D. (2008). Regional grey matter atrophy in clinically isolated syndromes at presentation. *Journal of Neurology, Neurosurgery, and Psychiatry*, 79, 1236–1244.
- Hernández-Torres, E., Wiggermann, V., Machan, L., Sadovnick, A. D., Li, D. K. B., Traboulsee, A., ... Rauscher, A. (2019). Increased mean R2* in the deep gray matter of multiple sclerosis patients: Have we been measuring atrophy? *Journal of Magnetic Resonance Imaging*, 50, 201–208.
- Hill, J. M., & Switzer, R. C., III. (1984). The regional distribution and cellular localization of iron in the rat brain. *Neuroscience*, 11, 595–603.
- Khalil, M., Langkammer, C., Pichler, A., Pinter, D., Gatteringer, T., Bachmaier, G., ... Fazekas, F. (2015). Dynamics of brain iron levels in multiple sclerosis: A longitudinal 3T MRI study. *Neurology*, 84, 2396–2402.
- Kutzelnigg, A., Lucchinetti, C. F., Stadelmann, C., Brück, W., Rauschka, H., Bergmann, M., ... Lassmann, H. (2005). Cortical demyelination and diffuse white matter injury in multiple sclerosis. *Brain*, 128, 2705–2712.
- Lane, D. J. R., Merlot, A. M., Huang, M. L.-H., Bae, D.-H., Jansson, P. J., Sahni, S., ... Richardson, D. R. (2015). Cellular iron uptake, trafficking and metabolism: Key molecules and mechanisms and their roles in disease. *Biochimica et Biophysica Acta - Molecular Cell Research*, 1853, 1130–1144.
- Langkammer, C., Krebs, N., Goessler, W., Scheurer, E., Ebner, F., Yen, K., ... Ropele, S. (2010). Quantitative MR imaging of brain iron: A postmortem validation study. *Radiology*, 257, 455–462.
- Langkammer, C., Liu, T., Khalil, M., Enzinger, C., Jehna, M., Fuchs, S., ... Ropele, S. (2013). Quantitative susceptibility mapping in multiple sclerosis. *Radiology*, 267, 551–559.
- Langkammer, C., Schweser, F., Krebs, N., Deistung, A., Goessler, W., Scheurer, E., ... Reichenbach, J. R. (2012). Quantitative susceptibility mapping (QSM) as a means to measure brain iron? A post mortem validation study. *NeuroImage*, 62, 1593–1599.
- Laule, C., Pavlova, V., Leung, E., Zhao, G., MacKay, A. L., Kozlowski, P., ... Moore, G. R. W. (2013). Diffusely abnormal white matter in multiple sclerosis: Further histologic studies provide evidence for a primary lipid abnormality with neurodegeneration. *Journal of Neuropathology and Experimental Neurology*, 72, 42–52.
- Li, X., Chen, L., Kutten, K., Ceritoglu, C., Li, Y., Kang, N., ... Faria, A. V. (2019). Multi-atlas tool for automated segmentation of brain gray matter nuclei and quantification of their magnetic susceptibility. *NeuroImage*, 191, 337–349.
- Lorio, S., Lutti, A., Kherif, F., Ruef, A., Dukart, J., Chowdhury, R., ... Draganski, B. (2014). Disentangling in vivo the effects of iron content and atrophy on the ageing human brain. *NeuroImage*, 103, 280–289.
- Louapre, C., Govindarajan, S. T., Gianni, C., Madigan, N., Sloane, J. A., Treaba, C. A., ... Mainero, C. (2017). Heterogeneous pathological processes account for thalamic degeneration in multiple sclerosis: Insights from 7 T imaging. *Multiple Sclerosis Journal*, 24(11), 1433–1444. <https://doi.org/10.1177/1352458517726382>.
- Meguro, R., Asano, Y., Odagiri, S., Li, C., & Shoumura, K. (2008). Cellular and subcellular localizations of nonheme ferric and ferrous iron in the rat brain: A light and electron microscopic study by the perfusion-Perls and -Turnbull methods. *Archives of Histology and Cytology*, 71, 205–222.
- Ndayisaba, A., Kaindstorfer, C., & Wenning, G. K. (2019). Iron in neurodegeneration—Cause or consequence? *Frontiers in Neuroscience*, 13, 180.
- Paling, D., Tozer, D., Wheeler-Kingshott, C. A. M., Kapoor, R., Miller, D. H., & Golay, X. (2012). Reduced R2' in multiple sclerosis normal appearing white matter and lesions may reflect decreased myelin and iron content. *Journal of Neurology, Neurosurgery, and Psychiatry*, 83, 785–792.
- Patenaude, B., Smith, S. M., Kennedy, D. N., & Jenkinson, M. (2011). A Bayesian model of shape and appearance for subcortical brain segmentation. *NeuroImage*, 56, 907–922.

- Paul, B. T., Manz, D. H., Torti, F. M., & Torti, S. V. (2017). Mitochondria and iron: Current questions. *Expert Review of Hematology*, 10, 65–79.
- Pontillo, G., Coccozza, S., Lanzillo, R., Russo, C., Stasi, M. D., Paoletta, C., ... Brunetti, A. (2019). Determinants of deep gray matter atrophy in multiple sclerosis: A multimodal MRI study. *American Journal of Neuroradiology*, 40, 99–106.
- Popescu, B. F., Frischer, J. M., Webb, S. M., Tham, M., Adiele, R. C., Robinson, C. A., ... Lucchinetti, C. F. (2017). Pathogenic implications of distinct patterns of iron and zinc in chronic MS lesions. *Acta Neuropathologica*, 134, 45–64.
- Schweser, F., Raffaini Duarte Martins, A. L., Hagemeyer, J., Lin, F., Hanspach, J., Weinstock-Guttman, B., ... Zivadinov, R. (2018). Mapping of thalamic magnetic susceptibility in multiple sclerosis indicates decreasing iron with disease duration: A proposed mechanistic relationship between inflammation and oligodendrocyte vitality. *NeuroImage*, 167, 438–452.
- Simons, M., & Nave, K.-A. (2016). Oligodendrocytes: Myelination and axonal support. *Cold Spring Harbor Perspectives in Biology*, 8, a020479.
- Stankiewicz, J. M., Neema, M., & Ceccarelli, A. (2014). Iron and multiple sclerosis. *Neurobiology of Aging*, 35, S51–S58.
- Stüber, C., Pitt, D., & Wang, Y. (2016). Iron in multiple sclerosis and its noninvasive imaging with quantitative susceptibility mapping. *International Journal of Molecular Sciences*, 17, 100.
- Taegle, Y., Hagemeyer, J., Bergsland, N., Dwyer, M. G., Weinstock-Guttman, B., Zivadinov, R., & Schweser, F. (2019). Assessment of mesoscopic properties of deep gray matter iron through a model-based simultaneous analysis of magnetic susceptibility and R2*—A pilot study in patients with multiple sclerosis and normal controls. *NeuroImage*, 186, 308–320.
- Takasaki, C., Yamasaki, M., Uchigashima, M., Konno, K., Yanagawa, Y., & Watanabe, M. (2010). Cytochemical and cytological properties of perineuronal oligodendrocytes in the mouse cortex. *The European Journal of Neuroscience*, 32, 1326–1336.
- Uddin, M. N., Lebel, R. M., Seres, P., Blevins, G., & Wilman, A. H. (2016). Spin echo transverse relaxation and atrophy in multiple sclerosis deep gray matter: A two-year longitudinal study. *Multiple Sclerosis*, 22, 1133–1143.
- Vavasour, I. M., Laule, C., Li, D. K. B., Traboulsee, A. L., & MacKay, A. L. (2011). Is the magnetization transfer ratio a marker for myelin in multiple sclerosis? *Journal of Magnetic Resonance Imaging*, 33, 710–718.
- Vercellino, M., Masera, S., Lorenzatti, M., Condello, C., Merola, A., Mattioda, A., ... Cavalla, P. (2009). Demyelination, inflammation, and neurodegeneration in multiple sclerosis deep gray matter. *Journal of Neuropathology and Experimental Neurology*, 68, 489–502.
- Verkhatsky, A. (2013). Oligodendrocytes. In *Glial physiology and pathophysiology* (pp. 245–319). Chichester, England: John Wiley & Sons. <https://doi.org/10.1002/9781118402061.ch5>
- Williams, R., Buchheit, C. L., Berman, N. E. J., & LeVine, S. M. (2012). Pathogenic implications of iron accumulation in multiple sclerosis. *Journal of Neurochemistry*, 120, 7–25.
- Yao, B., Bagnato, F., Matsuura, E., Merkle, H., van Gelderen, P., Cantor, F. K., & Duyn, J. H. (2012). Chronic multiple sclerosis lesions: Characterization with high-field-strength MR imaging. *Radiology*, 262, 206–215.
- Yao, B., Hametner, S., Gelderen, P. V., Merkle, H., Chen, C., Lassmann, H., ... Bagnato, F. (2014). 7 Tesla magnetic resonance imaging to detect cortical pathology in multiple sclerosis. *PLoS One*, 9, e108863.
- Yu, F. F., Chiang, F. L., Stephens, N., Huang, S. Y., Bilgic, B., Tantiwongkosi, B., & Romero, R. (2018). Characterization of normal-appearing white matter in multiple sclerosis using quantitative susceptibility mapping in conjunction with diffusion tensor imaging. *Neuroradiology*, 61, 71–79. <https://doi.org/10.1007/s00234-018-2137-7>
- Zecca, L., Youdim, M. B. H., Riederer, P., Connor, J. R., & Crichton, R. R. (2004). Iron, brain ageing and neurodegenerative disorders. *Nature Reviews Neuroscience*, 5, 863–873.
- Zivadinov, R., Havrdová, E., Bergsland, N. P., Tyblova, M., Hagemeyer, J., Seidl, Z., ... Horáková, D. (2013). Thalamic atrophy is associated with development of clinically definite multiple sclerosis. *Radiology*, 268, 831–841.
- Zivadinov, R., Tavazzi, E., Bergsland, N., Hagemeyer, J., Lin, F., Dwyer, M. G., ... Schweser, F. (2018). Brain iron at quantitative MRI is associated with disability in multiple sclerosis. *Radiology*, 289, 487–496.

SUPPORTING INFORMATION

Additional supporting information may be found online in the Supporting Information section at the end of this article.

How to cite this article: Schweser F, Hagemeyer J, Dwyer MG, et al. Decreasing brain iron in multiple sclerosis: The difference between concentration and content in iron MRI. *Hum Brain Mapp*. 2021;42:1463–1474. <https://doi.org/10.1002/hbm.25306>